ELSEVIER

Contents lists available at ScienceDirect

Synthetic Metals

journal homepage: www.elsevier.com/locate/synmet





Experimental and biophysical interaction studies of alanine modified polyaniline with bovine serum albumin and human serum albumin: Influence of alanine modification on the spectral, morphological and electronic properties

Ufana Riaz a,b,*, Nuzhat Nabi b, Faith R. Nwanze a, Fei Yan a

- a Department of Chemistry and Biochemistry, North Carolina Central University, NC, 27707, USA
- ^b Materials Research Laboratory, Department of Chemistry, Jamia Millia Islamia, New Delhi 110025, India

ARTICLE INFO

Keywords:
Polyaniline
Biophysical interaction
Morphology
Fluorescence

ABSTRACT

The present work reports for the first time, modification of aniline with alanine (Ala) in mole ratios of 80–20, 50–50 and 20–80 via ultrasound-assisted polymerization. The formation of Ala-incorporated polyaniline (PANI) was confirmed via FTIR, UV–visible and SEM studies. The geometry optimization, Mulliken charge distribution, vibrational as well as electronic spectral analysis was carried out using Gaussian 09 software with B3LYP/6311 G (d) basis set. Quenching of bovine serum albumin (BSA) and human serum albumin (HSA) by Ala/PANI followed the static mechanism which was confirmed by the fluorescence studies and Stern Volmer plots. The binding constant (K_b) values were found to be higher for Ala-PANI oligomers ($\sim 10^5 \, \text{LM}^{-1}$) containing higher loading of PANI. The binding affinity of Ala/PANI towards BSA as well as HSA was found to be fairly good and the docking studies established that hydrogen bonding as well as Van der Waal's forces played a significant role in the binding process.

1. Introduction

Conducting polymers such as polyacetylene (PAc) [1], polyaniline (PANI) [2], poly(1-naphthylamine) (PNA) [3,4], poly (o-phenylenediamine) (POPD) [5,6], polypyrrole (PPy) [7,8] etc. have exceptional electro-active and optoelectronic features which can be easily modified to obtain functional polymers having potential application in the fields of photocatalysis [9–11], biosensors [12–14], drug delivery [15,16] and corrosion protection [17,18]. Among all, PANI has exceptional properties due to its pH-responsive characteristics and the ability to exist in different conducting as well as insulating states in acidic, basic and neutral media.

Amino acids such as (Ala), asparagine (Asn), glutamine (Gln), histidine (His), Isoleucine (Ile), lysine (Lys), proline (Pro), threonine (Thr), and valine (Val) etc. are known to increase the biocompatibility of materials and have been incorporated in several synthetic/natural polymers to enhance their sensing characteristics. For designing polymers applicable in protein detection/sensing, various methods have been used to immobilize bioreceptors on the polymeric surface. Since

PANI is synthesized under highly acidic solutions conditions (pH 0–2), immobilization by covalent methods is usually adopted to avoid leaching of the receptor molecules. Studies dealing with biocompatibility of PANI have been extensively investigated by *Mattioli and Belmonte* et al. [19] using the in-vivo testing as well as in-vitro proliferation of cells on PANI surfaces [20]. Application of Ala-based complex isomers for the detection of heavy metal ions (HMIs) has been reported by Akhtar and co-workers [21]. *Han and Chi* [22] reported the complex formation and capability of various α -amino acids with Fe(II), Fe(III), Cu(II), and Zn(II) for the detection of metal ions.

Although a lot of work has been reported on the interaction of amino acids with conducting polymers, no quantitative work has been reported on the influence of Ala concentration on the conformational changes in PANI and its interaction with bovine serum albumin (BSA) as well as human serum albumin (HSA) [23,24]. Hence, with a view to explore the effect of Ala-incorporated PANI on the optoelectronic as well as biophysical interaction potential with BSA and HSA, the present work reports ultrasound-assisted polymerization of aniline and its modification with Ala in the mol ratios of 80–20,50–50 and 20–80 respectively. The

^{*} Corresponding author at: Department of Chemistry and Biochemistry, North Carolina Central University, NC, 27707, USA. *E-mail addresses*: ufana2002@yahoo.co.in, uriaz@nccu.edu (U. Riaz).

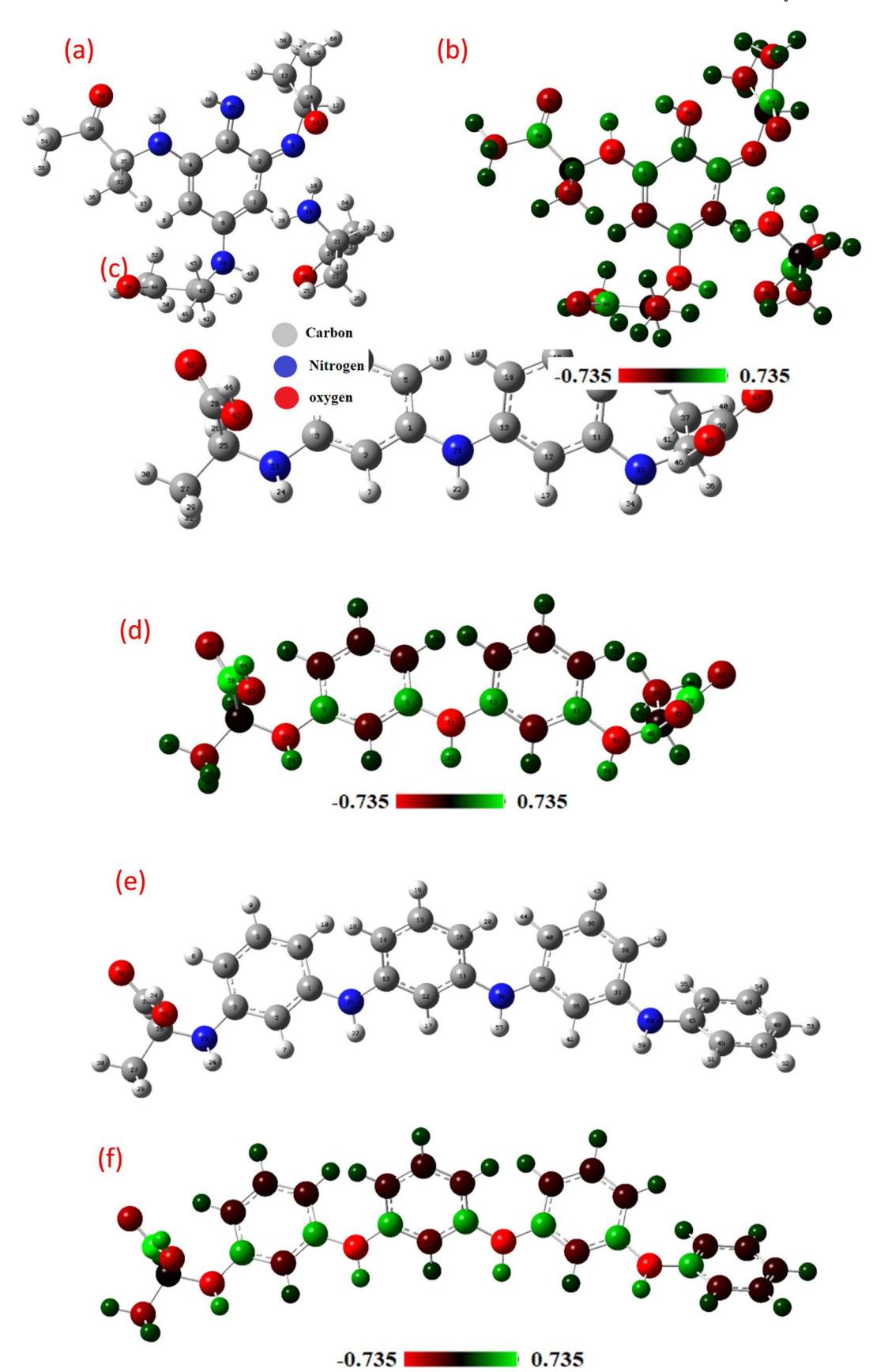


Fig. 1. (a) Geometry optimized structure of Ala-PANI/80–20, (b) Mulliken charge distribution in Ala-PANI/80–20,(c) geometry optimized structure of Ala-PANI/50–50, (d) Mulliken charge distribution in Ala-PANI/20–80, (e) geometry optimized structure of Ala-PANI/20–80, (f) Mulliken charge distribution in Ala-PANI/20–80.

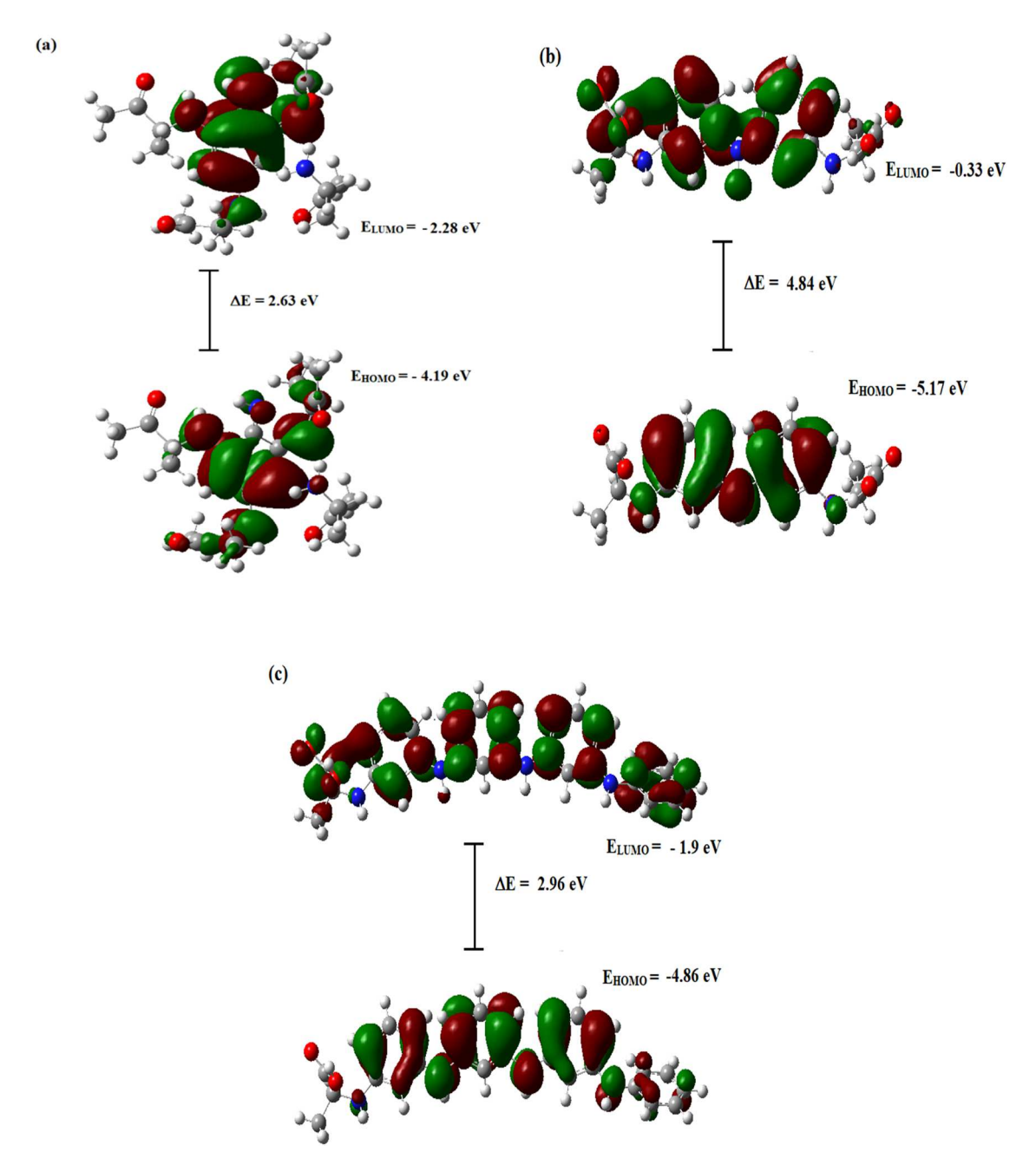


Fig. 2. Frontier molecular orbital distributions in (a) Ala-PANI/80–20, (b) Ala-PANI/50–50, (c) Ala-PANI/20–80.

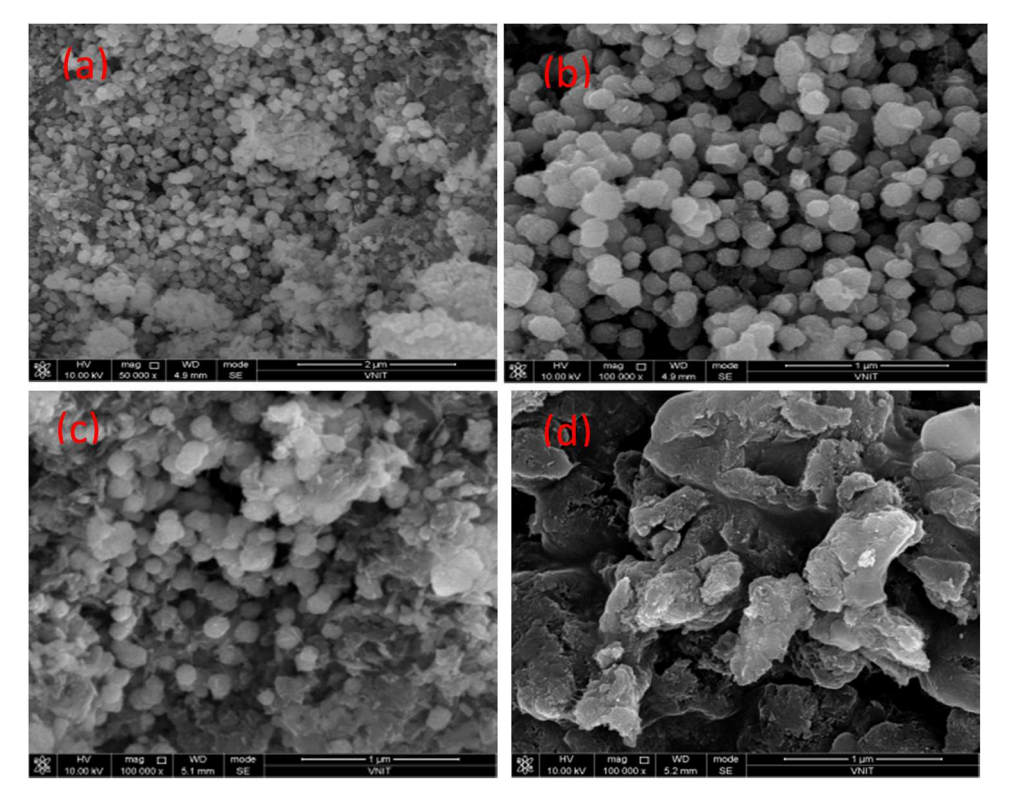


Fig. 3. SEM of (a) PANI, (b), Ala-PANI/80-20, (c) Ala-PANI/50-50, (d) Ala-PANI/20-80.

synthesized polymers were investigated for their spectroscopic and morphological properties. The theoretical studies were computed with B3LYP/6311 G(d) basis set using Gaussian 09 software. The optimized geometries, band gap as well as the theoretical IR and UV spectra were compared with the experimental findings to establish the incorporation of Ala in PANI.

2. Experimental

Aniline (Sigma Aldrich, USA), Alanine (Loba Chemie, India), ferric chloride (FeCl $_3$ -6 H $_2$ O, Sd Fine Chem Pvt. Ltd, India), HCl (Merck, India), ethanol (Merck, India), dimethyl-formamide (DMF) (Sd. Fine Chem., Pvt. Ltd, India), were used as received.

2.1. Synthesis of polyaniline (PANI)

Aniline (0.2 M, 9 ml) was added to a 150 ml conical flask containing HCl and was stirred on a magnetic stirrer at 0 $^{\circ}$ C. The oxidant FeCl₃ (4 g) was added to the above mixture under constant stirring and the solution was further stirred for 2 h at the same temperature. The black precipitate of PANI was then centrifuged and kept in vacuum oven at 70 $^{\circ}$ C for 48 h to ensure complete removal of water. The yield obtained was 1.6 g.

2.2. Incorporation of alanine in PANI

Alanine (0.5 g) was dissolved in deionized water (100 ml) and added to the solution of PANI prepared by dissolving 0.5 g in 10 ml DMF. The reaction mixture was sonicated for 2 h at 20 °C. The product obtained was centrifuged and kept in vacuum oven at 70 °C for 48 h to ensure complete removal of water. The sample was designated as Ala-PANI/50–50. Similar method was adopted to synthesize Ala/PANI in the mol ratios of 80–20 and 20–80 and were designated as Ala-PANI/80–20 and Ala-PANI/20–80 respectively. The percent yield obtained was as follows: Ala-PANI/50–50: 75%; Ala-PANI/80–20: 78%, PANI/20–80:80%.

3. Characterization

3.1. Spectral studies

IR spectra was recorded on FT-IR spectrophotometer Shimadzu, Model IRA Affinity-1. The UV-visible spectra were taken on UV-vis spectrophotometer model Shimadzu, UV-1800 in DMF. Fluorescence studies were performed on fluorescence spectrophotometer Fluorolog@ 3–11 using water as solvent.

3.2. Morphological studies

TEM micrographs (TEM) were acquired using the Morgagni Model 268-D TEM system (FEI, USA).

3.3. Theoretical studies

DFT and TD-DFT calculations were performed using GAUSSIAN 09 software, and the optimized geometries were obtained using DFT/B3LYP using 6–311 G(d) basis set [25,26]. The oscillator strength, HOMO-LUMO energies, band gap, vibrational frequency calculations and UV—vis spectra were determined using the optimized geometries by applying the same basis set.

3.4. Interaction studies with bovine serum albumin

For BSA interaction studies, Ala-PANI solution $(2.0\times10^{-5} \text{ M})$ was prepared in phosphate buffer solution (PBS, pH=7.4) as per reported method [23]. The stock solution of BSA $(5\times10^{-6} \text{ M})$ was prepared by dissolving an appropriate amount of BSA in PBS. BSA $(0.35 \text{ ml}, 5\times10^{-6} \text{ M})$ was mixed with 0.05–0.30 ml of Ala-PANI, and the solutions were shaken for 30 min on an orbital shaker at 25 °C. The fluorescence emission spectra were recorded in the wavelength range of 280–550 nm on a fluorescence spectrophotometer model Fluorolog®3, Horiba

Table 1Experimental and theoretical IR data of Ala-PANI oligomers.

Sample polymers	Functional group	Experimental Peak Position	Theoretical peak position
PANI	NH stretching	3151	_
	C-H stretching (aromatic /aliphatic)	2954, 2850	-
	Imine stretching	1651	-
	C=C stretching (quinonoid)	1560, 1480	-
	C=C stretching (benzenoid)	1408,1400	-
	C-N stretching	1242	-
	Substituted phenyl ring	979,742,682	-
Ala-PANI/80-20	NH stretching (aniline)	3126	3163
	NH stretching (alanine)	3024	3064
	C=O stretching	1774	1786
	Imine stretching	1645	1651
	C=C stretching (quinonoid)	1585	1588,1543,1534
	C=C stretching (benzenoid)	1402,1342	1408,1399,1345
	C-N stretching	1265	1255
	Substituted phenyl ring	879,790,680	976,877,760,680
Ala-PANI/50–50	NH stretching (aniline)	3122	3172
	NH stretching (alanine)	3024	3073,3037
	C=O stretching	1745	1750
	Imine stretching	1689	1651
	C=C stretching (quinonoid)	1587, 1564,1544	1579,1570,1534,
	0.11	• •	1462,1453
	C=C stretching (benzenoid)	1390,1342,1307	1372,1363,1327,
	0 (1 1 1 1)	,,	1309
	C-N stretching	1267	1264
	Substituted phenyl ring	956, 790,680	976,814,778,670,652
Ala-PANI/20–80	NH stretching (aniline)	3126	3127
	NH stretching (alanine)	3024	3064
	C=O stretching	1774	1768
	Imine stretching	1645	1642
	C=C stretching (quinonoid)	1585, 1402	1597,1588,1471,
	0.11	•	1444
	C=C stretching (benzenoid)	1342,1300	1372,1363,1345
	C-N stretching	1265	1264
	Substituted phenyl ring	879,790,680	976,931,796,670

Scientific. Rayleigh Light scattering (RLS) measurements were performed via simultaneously scanning the excitation and emission monochromators of the spectrofluorometer from 50 nm to 400 nm with $\Delta\lambda=0$ nm and a slit width of 1.5 nm. For circular dichroism (CD) measurements, BSA dissolved in PBS (0.5 ml, 5.0 $\times 10^{-6}$ M) taken as control and was mixed with 2.5 ml of Ala/PANI. The measurements were taken in the UV region in the wavelength range of 195 nm - 230 nm with band width of 5 nm on a Jasco-815 automatic recording spectro-polarimeter (Japan) at room temperature using a cell of 2 mm path length.

3.5. Molecular docking

The 3-dimesional X-ray structures of BSA (encoded 3V03) and HSA (encoded 1AO6) were obtained from the Brookhaven Protein Data Bank (http://www.pdb.org). The optimized complexes were considered for docking study. Auto Dock 4.2 suite molecular-docking tool was utilized for the docking analysis. The binding position, bound conformation of Ala/PANI with the BSA/HSA along with the rough estimate of their interactions were examined using Auto Dock software. To analyze the mode of binding, docked conformation at the lowest binding energy was selected [24–27].

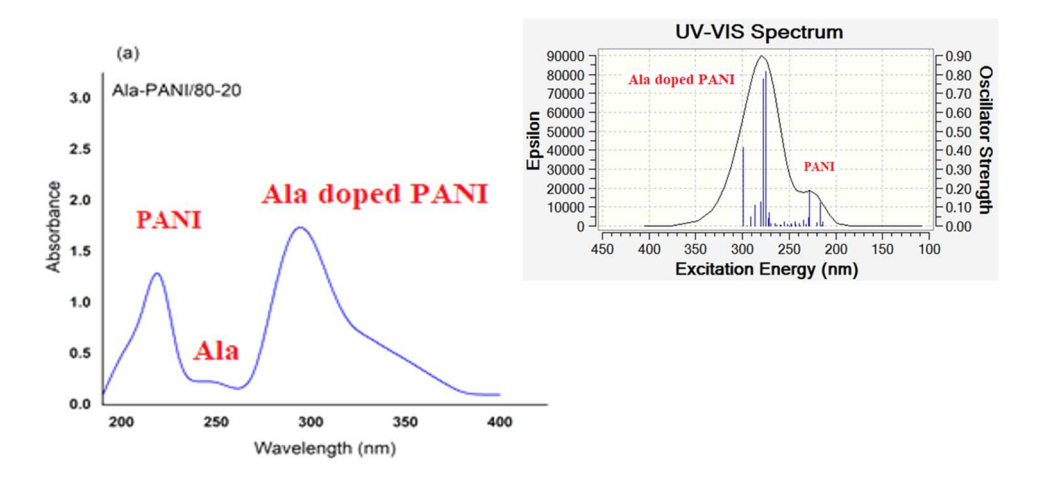
4. Results and discussion

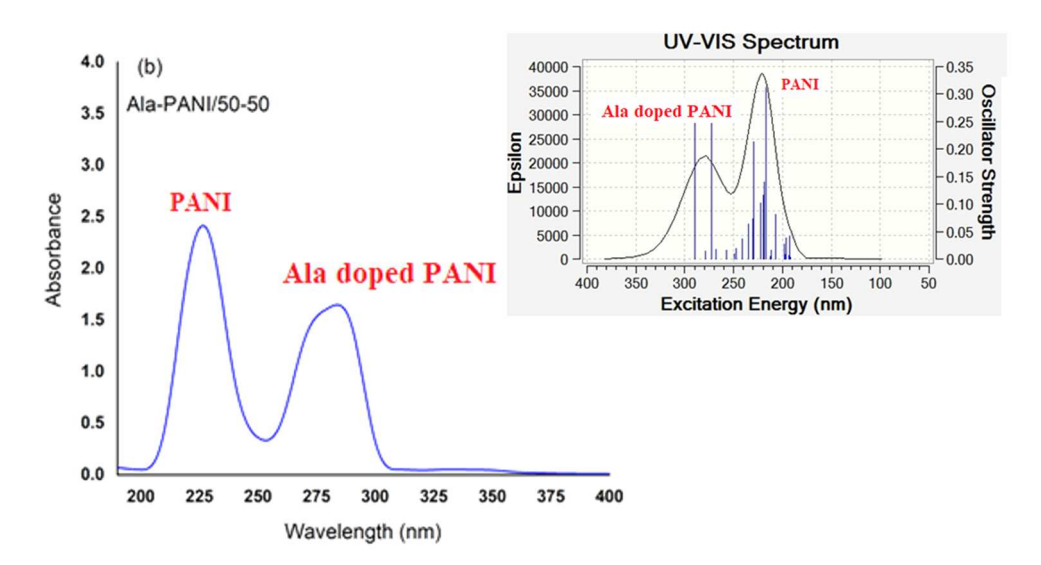
The viscosity molecular weight was determined as per the protocol reported in our earlier studies [23,24]. The viscosity average molecular weights M_{ν} were obtained as 5537, 4620, 5823 for Ala-PANI/80–20, Ala-PANI/50–50, and Ala-PANI/20–80 respectively, which confirmed formation of oligomers. Hence, the geometries for Ala-PANI/80–20, Ala-PANI/50–50, and Ala-PANI/20–80 were optimized by taking 4 units

of alanine and one monomer unit of aniline, 2 units of alanine and 2 units of aniline and 1 unit of alanine and 4 units of aniline respectively. The geometry optimized structures of alanine incorporated PANI are depicted in Fig. 1(a-f).

The oligomer of Ala-PANI/80–20, Fig. 1(a), showed twisting of Ala units around the aniline monomer unit. The charge was observed to be concentrated around the NH and oxygen of C=O bonds, Fig. 1(a). For the Ala-PANI/50/50, the Ala units at the terminals of the aniline dimer showed twisting and distortion of the planar configuration, Fig. 1(c). The charge was noticed to be concentrated around the NH units of aniline, Ala as well as around the oxygen of C=O unit of Ala, Fig. 1(d). The charge density was found to be intense around oxygen of C=O unit due to its electron with-drawing nature, while in case of the NH units, the increase in the charge density was attributed to intense charge transfer between the amino nitrogen of the benzenoid rings. In case of Ala-PANI/ – 20–80, the terminal aniline unit was found to undergo distortion, while the rest of the 3 aniline units were observed to be planar, Fig. 1(e). The charge in this case too was found to be centered on the NH as well as the C=O units of Ala, Fig. 1(f).

The highest occupied molecular orbitals (HOMO) and the lowest unoccupied molecular orbitals (LUMO) were noticed to be delocalized around the aniline monomer, Fig. 2(a), with high charge delocalization around the C=O as well as NH groups. The band gap was calculated to be 2.63 eV. For Ala-PANI/50–50, Fig. 2(b), the LUMO orbitals were noticed to be concentrated around the aniline dimer and the band gap was computed to be 4.84 eV, while for Ala-PANI/20–80, Fig. 2(c), the band was computed to be 2.96 eV. The LUMO as well as HOMO orbitals were homogeneously distributed over the aniline units.





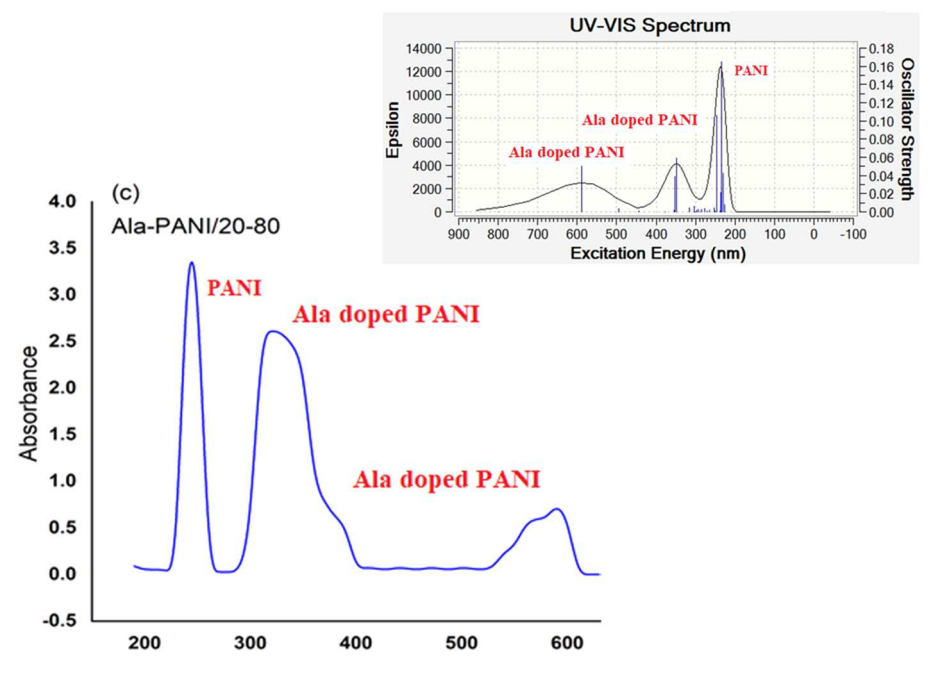
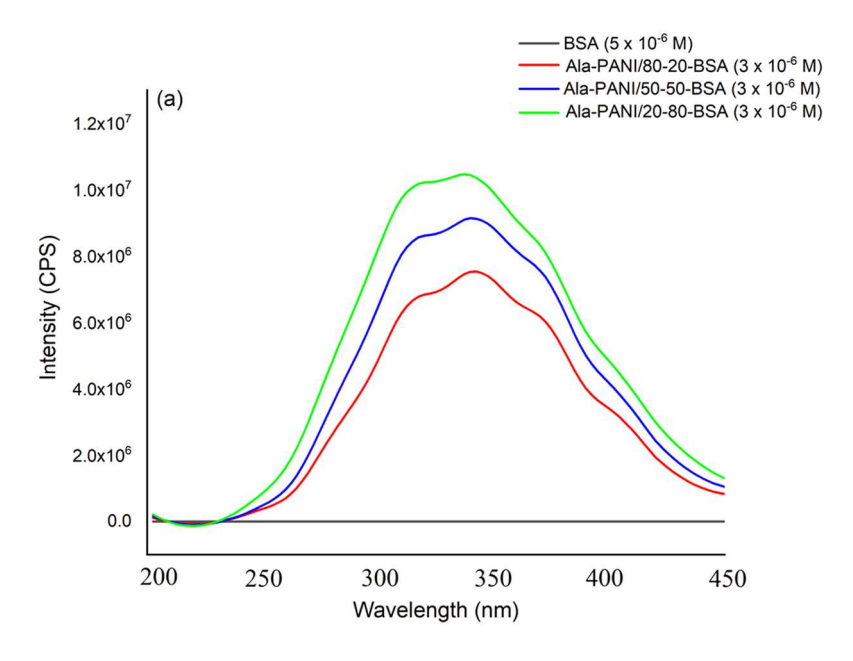


Fig. 4. UV-visible spectra of (a) Ala-PANI/80-20, (c) Ala-PANI/50-50, (d) Ala-PANI/20-80.



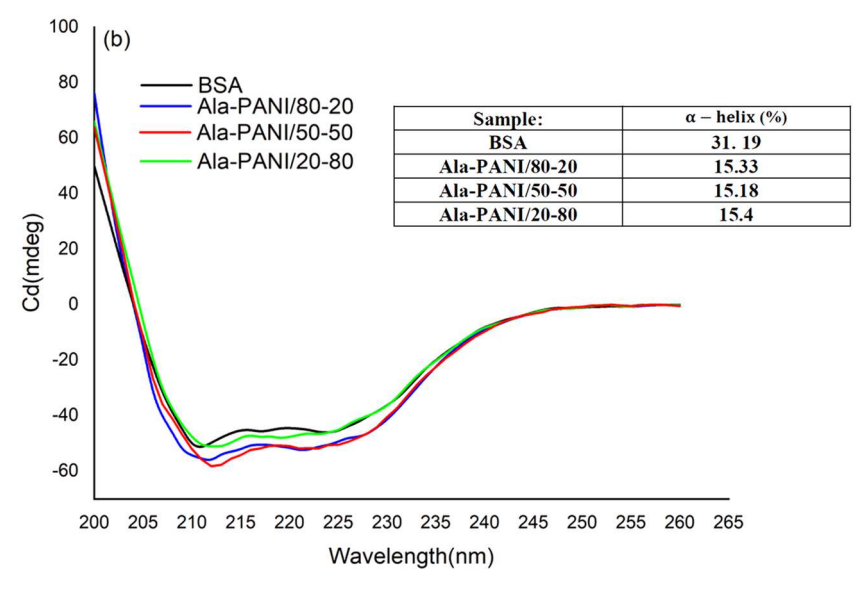


Fig. 5. (a) RLS profile of Ala-PANI/80-20, Ala-PANI/50-50, Ala-PANI/20-80 (b) CD profile of Ala-PANI/80-20, Ala-PANI/50-50, Ala-PANI/20-80.

4.1. Morphological studies

The SEM of pristine PANI, Fig. 3(a), showed formation of homogeneous globular structures similar to the ones noticed in a cauliflower. The SEM of Ala-PANI/80–20, Fig. 3(b), revealed the formation of homogeneous spherical morphology comprising of large globular particles, while the SEM of Ala-PANI/80–20, Fig. 3(c), exhibited a mixed morphology of spherical globules and fibrillar particles, Fig. 3(c). The SEM of Ala-PANI/20–80, Fig. 3(d) showed the formation of flaky particles reflecting a crystalline morphology. The SEM images clearly showed the effect of incorporation of Ala in PANI on the morphological characteristics which showed variation as per the concentration of Ala in PANI.

4.2. Spectral analysis

The IR spectrum of pristine PANI revealed an NH stretching vibration

peak at 3151 cm⁻¹, while the imine stretching vibration peak was noticed at 1651 cm⁻¹, Table 1 (given in supporting information as Fig. S1). The benzenoid and quinonoid ring stretching vibration peaks were noticed at 1560 cm⁻¹, 1480 cm⁻¹, 1408 cm⁻¹, 1400 cm⁻¹, while the CN stretching vibration peak was observed at 1242 cm⁻¹. The peaks associated with substituted aromatic rings were seen at 979 cm^{-1} ,742 cm⁻¹,682 cm⁻¹. The IR spectrum of Ala-PANI-80/20 showed the NH stretching vibration peak of PANI at 3126 cm⁻¹, while the NH stretching vibration peak associated with Ala was observed at 3024 cm⁻¹. The C=O stretching peak of Ala appeared at 1774 cm⁻¹ and the imine stretching peak was noticed at 1645 cm^{-1} . The quinonoid and benzenoid ring stretching peaks were observed at 1585 cm⁻¹, 1402 cm^{-1} , 1342 cm^{-1} . The CN stretching peak appeared at 1265 cm^{-1} . The theoretical IR spectrum of Ala-PANI-80/20 showed peak of NH of PANI at 3163 cm⁻¹, while the NH bending peak of Ala was noticed at 3064 cm⁻¹. The C=O stretching peak was observed at 1786 cm⁻¹ and the imine stretching peak was observed at 1651 cm⁻¹. The quinonoid

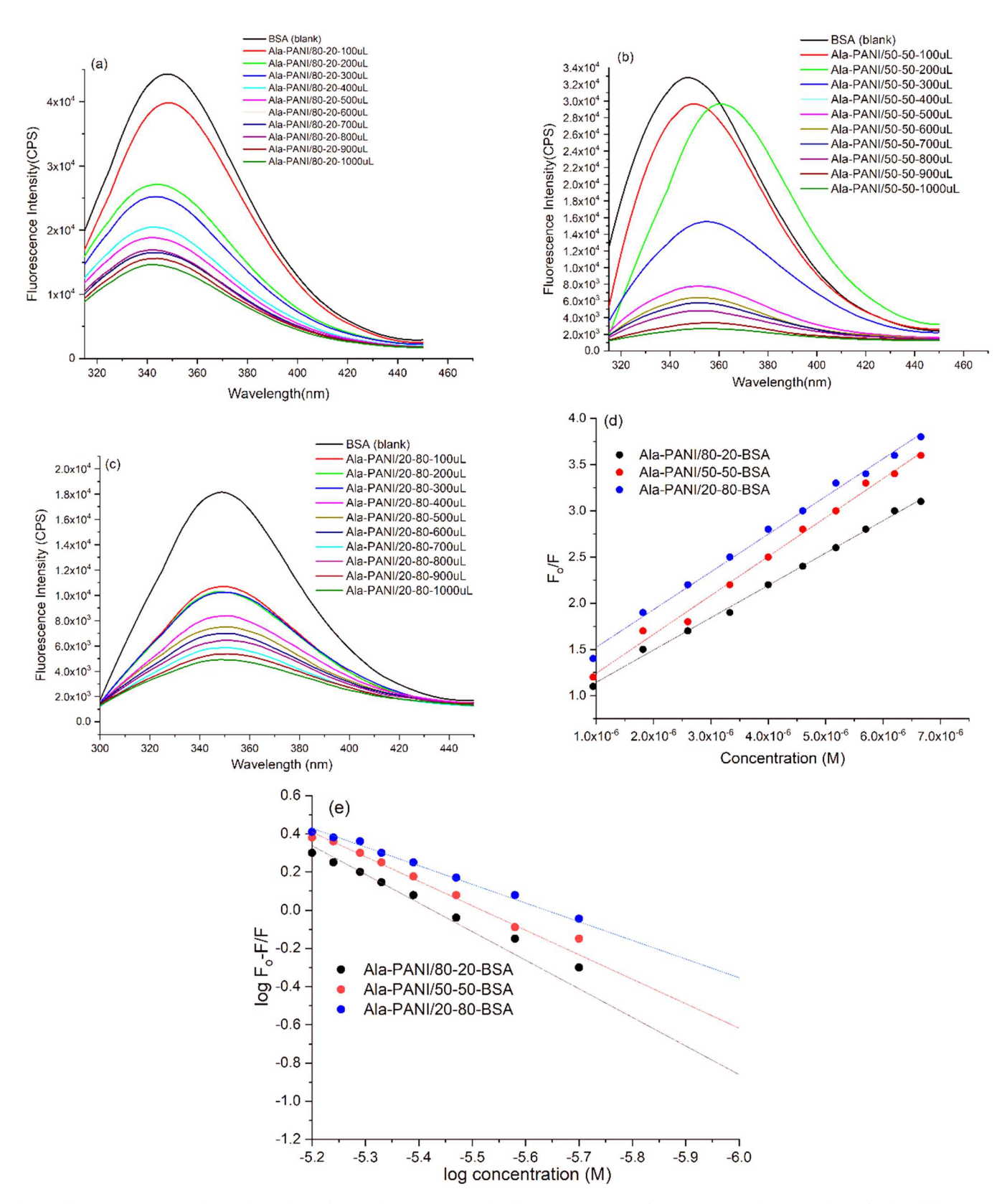


Fig. 6. Fluorescence spectra of quenching of BSA by (a) Ala-PANI/80–20, (b) Ala-PANI/50–50, (c) Ala-PANI/20–80, (d) Stern Volmer plot for of fluorescence quenching of BSA (e) plot of log F_0 -F/F vs log concentration.

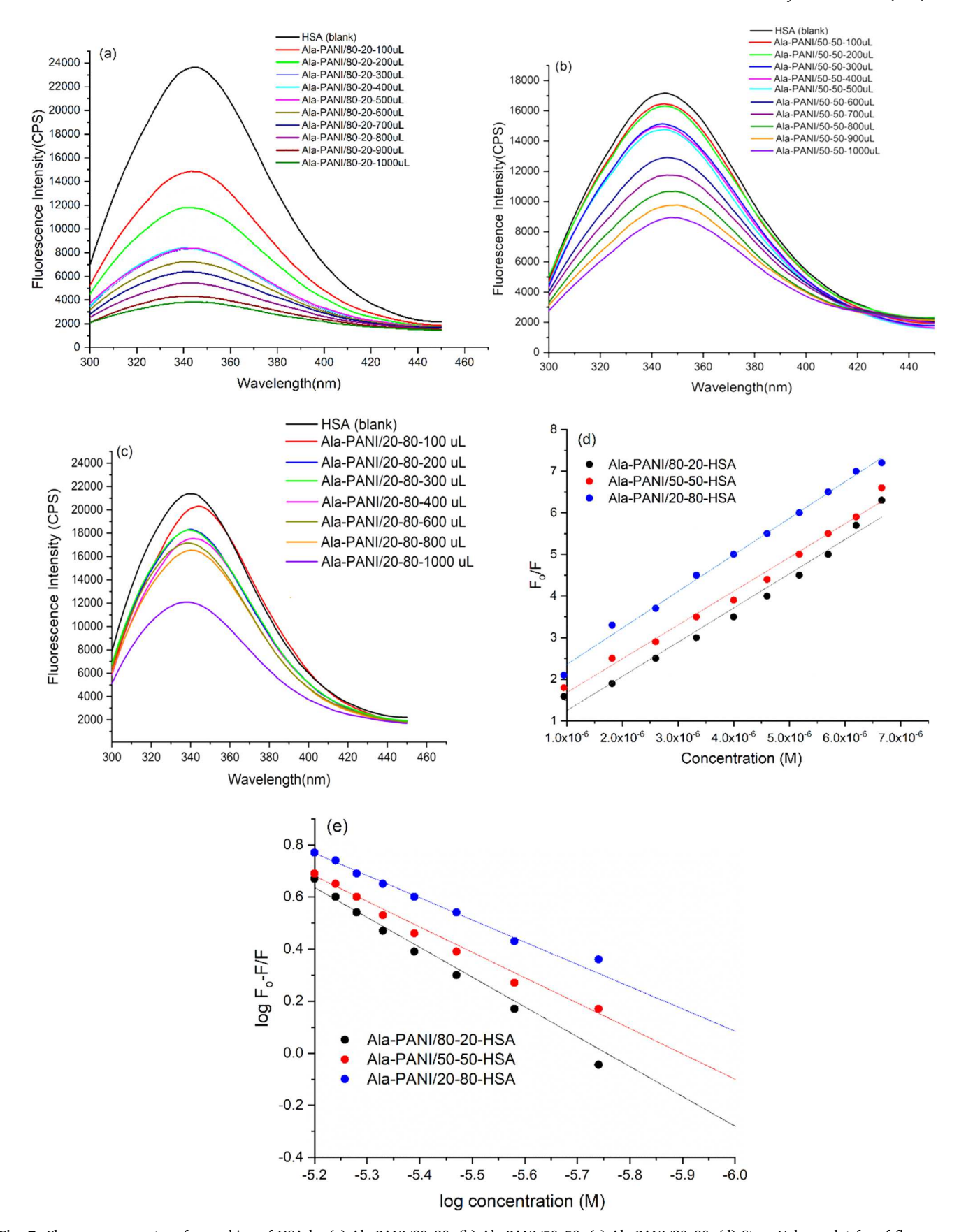


Fig. 7. Fluorescence spectra of quenching of HSA by (a) Ala-PANI/80–20, (b) Ala-PANI/50–50, (c) Ala-PANI/20–80, (d) Stern Volmer plot for of fluorescence quenching of BSA (e) plot of log F_0 - F_7 F vs log concentration.

Table 2
Stern vomer, quenching rate and binding rate constant values for Ala-PANI/80–20, Ala-PANI/50–50 and Ala-PANI/20–80 with BSA and HSA.

Polymer	quenching constant (K_{SV}) (LM^{-1})	bimolecular quenching rate (K_q) ($LM^{-1}\ s^{-1}$)	Binding constant value (K_a) (LM^{-1})	Binding sites
Ala-PANI/80-20-BSA	7.9×10^5	7.9×10^{13}	8.12×10^6	1.5
Ala-PANI/50-50-BSA	8.2×10^{5}	$8.2 imes 10^{13}$	7.90×10^{6}	1.3
Ala-PANI/20-80-BSA	1.1×10^{6}	1.1×10^{14}	$5.5 imes 10^{6}$	1
Ala-PANI/80-20-HSA	4.2×10^{5}	$4.2 imes 10^{13}$	$8.2 imes 10^6$	0.5
Ala-PANI/50-50-HSA	8.6×10^{5}	8.6×10^{13}	8.11×10^{6}	0.9
Ala-PANI/20-80-HSA	1.47×10^6	1.47×10^{14}	8.7×10^6	1

benzenoid ring stretching peaks were attained $1588 \ \mathrm{cm^{-1}}, 1543 \ \mathrm{cm^{-1}}, 1534 \ \mathrm{cm^{-1}}, \ \ 1408 \ \mathrm{cm^{-1}}, 1399 \ \mathrm{cm^{-1}}, 1345 \ \mathrm{cm^{-1}}$ and the CN stretching peak was noticed at 1255 cm⁻¹. The peaks were found to be in good agreement with the experimental spectra. Likewise. the IR spectrum of Ala-PANI-50/50 and Ala-PANI-20/80 exhibited the NH stretching vibration peaks at 3122 cm⁻¹, 3024 cm⁻¹, 3126 cm⁻¹ and 3024 cm⁻¹ respectively, while the theoretical spectra revealed the same peaks at 3172 cm^{-1} , 3073 cm^{-1} and 3037 cm^{-1} for Ala-PANI-50/ 50. For Ala-PANI-80/20, the NH stretching vibration peaks were noticed at 3127 cm⁻¹ and 3064 cm⁻¹. The C=O stretching peak was observed at $1745\;\text{cm}^{-1}$ for Ala-PANI-50/50 and in the theoretical spectrum, this peak appeared at 1750 cm⁻¹. The quinonoid and benzenoid stretching vibration peaks were noticed at 1587 cm⁻¹, 1564 cm⁻¹,1544 cm⁻¹ and 1390 cm^{-1} , 1342 cm^{-1} , 1307 cm^{-1} , whereas the theoretical spectra revealed these peaks at $1579~\mathrm{cm}^{-1}$, $1570~\mathrm{cm}^{-1}$, $1534~\mathrm{cm}^{-1}$, $1462~\mathrm{cm}^{-1}$, $1453~\mathrm{cm}^{-1}$, $1372~\mathrm{cm}^{-1}$, $1363~\mathrm{cm}^{-1}$, $1327~\mathrm{cm}^{-1}$ and 1309 cm⁻¹. The experimental spectrum of Ala-PANI-80/20 revealed the C=O stretching peak at 1774 cm⁻¹ and the theoretical spectrum exhibited this peak at 1768 cm⁻¹. The imine stretching peak was found at 1645 cm⁻¹in the experimental spectrum and at 1642 cm⁻¹ in the theoretical spectrum. The experimental and the theoretical spectra for all the alanine modified PANI polymers were in close agreement and thus confirmed the geometry optimized structures as depicted in Fig. 1.

The UV–visible spectrum of Ala-PANI/80–20, Fig. 4(a) exhibited two intense peaks at 239 nm and 310 nm due to the π - π * transitions associated with PANI as well as Al doped PANI. The theoretical spectrum showed the same transitions at 240 nm and 280 nm. The oscillator strength of the former peak was computed to be 0.90. The UV spectrum of Ala-PANI/50–50, Fig. 4(b), showed peaks at 225 nm, 280 nm in the UV range and the theoretical spectrum revealed the same peaks at 230 nm and 290 nm. The oscillator strength of the former peak was computed to be 0.35. The UV spectrum of Ala-PANI/80–20, Fig. 4(c), exhibited intense peaks at 225 nm, 330 and 575 nm and interestingly, the theoretical spectrum revealed these transitions at 230 nm, 330 nm and 600 nm. The later broad peak was associated with n- π * transition suggesting higher extent of conjugation in this polymer. It was noticed that the transitions were found to vary with the loading of Ala and were found to shift significantly with the increase in the Ala loading in PANI.

4.3. RLS and Circular dichroism (CD) studies

The RLS profile of BSA solution in presence of Ala-PANI-80/20, Fig. 5 (a), showed intense peak around 325 nm indicating the formation of aggregates. The RLS signal intensity of Ala-PANI-50/50, and Ala-PANI-20/80 showed much higher intensities as compared to the previous case. Formation of aggregates of larger sizes was therefore confirmed. Circular dichroism (CD) was carried out to explore the changes in secondary and tertiary structure of BSA upon interaction with Ala-PANI. The CD spectrum of BSA, Fig. 5(b), revealed bands at 208 nm and 222 nm in the UV region which were characteristic peaks associated with the of the α -helix structure of the protein [23,24].

The equation of MRE was used to calculate the alpha helix percentage by using the following formula: $\alpha - \text{helix}(\%) = [(-MRE_{210} - 4000)/(33,000 - 4000)] \times 100$.

Where MRE $_{210}$ the observed MRE value at 210 nm, 4000 is the MRE value for the β -sheet at 210 nm and 33,000 is the MRE value of pure α —helix at 210 nm.

The α -helix content of free BSA was computed to be 31.19% and was found to be of higher intensity than the one bound to Ala-PANI, Fig. 5 (b). The α -helix content was observed to decrease and was observed to be lowest for Ala-PANI/50–50. Interestingly, the CD spectrum of BSA in presence as well as in absence of Ala-PANI was observed to be of similar shape, indicating that the structure of BSA was predominantly α -helical even after binding with the oligomers. Since the amide groups present in Ala-PANI are hydrophobic, they tend to exist as coils in aqueous phase so as to minimize energy and penetrate into the polypeptide backbone of tryptophan-213. This has been reported by several authors [23,24].

4.4. UV and fluorescence quenching studies

The F_0/F vs [C] plots were analyzed to confirm the static/dynamic quenching in the synthesized oligomer complex with BSA/HSA [24]. The plot of F_0/F against [Q] is a straight line indicating that the quenching is not predominantly static in nature. The K_q was estimated using the Stern-Volmer equation:

$$F_0/F = 1 + k_a t_0[Q] = 1 + K_{sv}[Q]$$

Where F_0 and F are the intensities of fluorescence in absence and presence of the quencher, [Q] is the concentration of the quenching species. K_{SV} is the quenching constant which is also equivalent to kt_0 , with k_q known as the bimolecular quenching rate constant and t_0 as the lifetime of the sample (BSA) in absence of the quenching species(polymer).

The fluorescence intensity at 350 nm emission was found to show a decrease in the intensity upon addition of Ala-PANI/80–20, Ala-PANI/50–50, and Ala-PANI/20–80 in BSA as well as HSA, Fig. 6(a-c), Fig. 7(a-c). The quenching rate constant values (kq) were observed to be $7.9\times10^{13}\,\mathrm{LM^{-1}\,s^{-1}},8.2\times10^{13}\,\mathrm{LM^{-1}\,s^{-1}},1.1\times10^{14}\,\mathrm{LM^{-1}\,s^{-1}}$ for Ala-PANI/80–20-BSA, Ala-PANI/50–50-BSA, and Ala-PANI/20–80-BSA respectively, Table 2.

The K_{SV} values were found to be $7.9\times10^5~LM^{-1}$ for Ala-PANI/ $80\text{--}20\text{-BSA},~8.2\times10^5~LM^{-1}$ for Ala-PANI/50–50-BSA and $1.1\times10^6~LM^{-1}$ for Ala-PANI/20–80-BSA, Fig. 6(d). Similarly, the quenching rate constant values (k_q) were observed to be $4.2\times10^{13}~LM^{-1}~s^{-1},~8.6\times10^{13}~LM^{-1}~s^{-1}$ and $1.47\times10^{14}~LM^{-1}~s^{-1}$ for Ala-PANI/80–20-HSA, Ala-PANI/50–50-HSA, and Ala-PANI/20–80-HSA respectively.

The K_{SV} values were found to be $4.2\times10^5~LM^{-1}$ for Ala-PANI/ $80{\text -}20{\text -}HSA$, $8.6\times10^5~LM^{-1}$ for Ala-PANI/ $50{\text -}50{\text -}HSA$ and $1.47\times10^6~LM^{-1}$ for Ala-PANI/ $20{\text -}80{\text -}HSA$, Fig. 7(d). The values of quenching rate were fairly higher than the values obtained for biological macromolecules due to the collision mechanism (2.0 $\times10^{10}~LM^{-1}~s^{-1}$) which confirmed that the binding of BSA/HSA with Ala-PANI took place through static mechanism via the formation of an intermolecular complex. The binding constant value (K_a) was computed from the Stern-Volmer equation as reported in our previous studies[23]. The K_a value was calculated to be $8.12\times10^6~LM^{-1}$ with binding sites equal to 1.5 for Ala-PANI/ $80{\text -}20{\text -}BSA$ and $7.90\times10^6~LM^{-1}$ for Ala-PANI/ $50{\text -}50{\text -}BSA$ with binding sites equal to 1.3, Table 2. The K_a value was calculated to be $5.5\times10^6~LM^{-1}$ with binding sites equal to 1 for

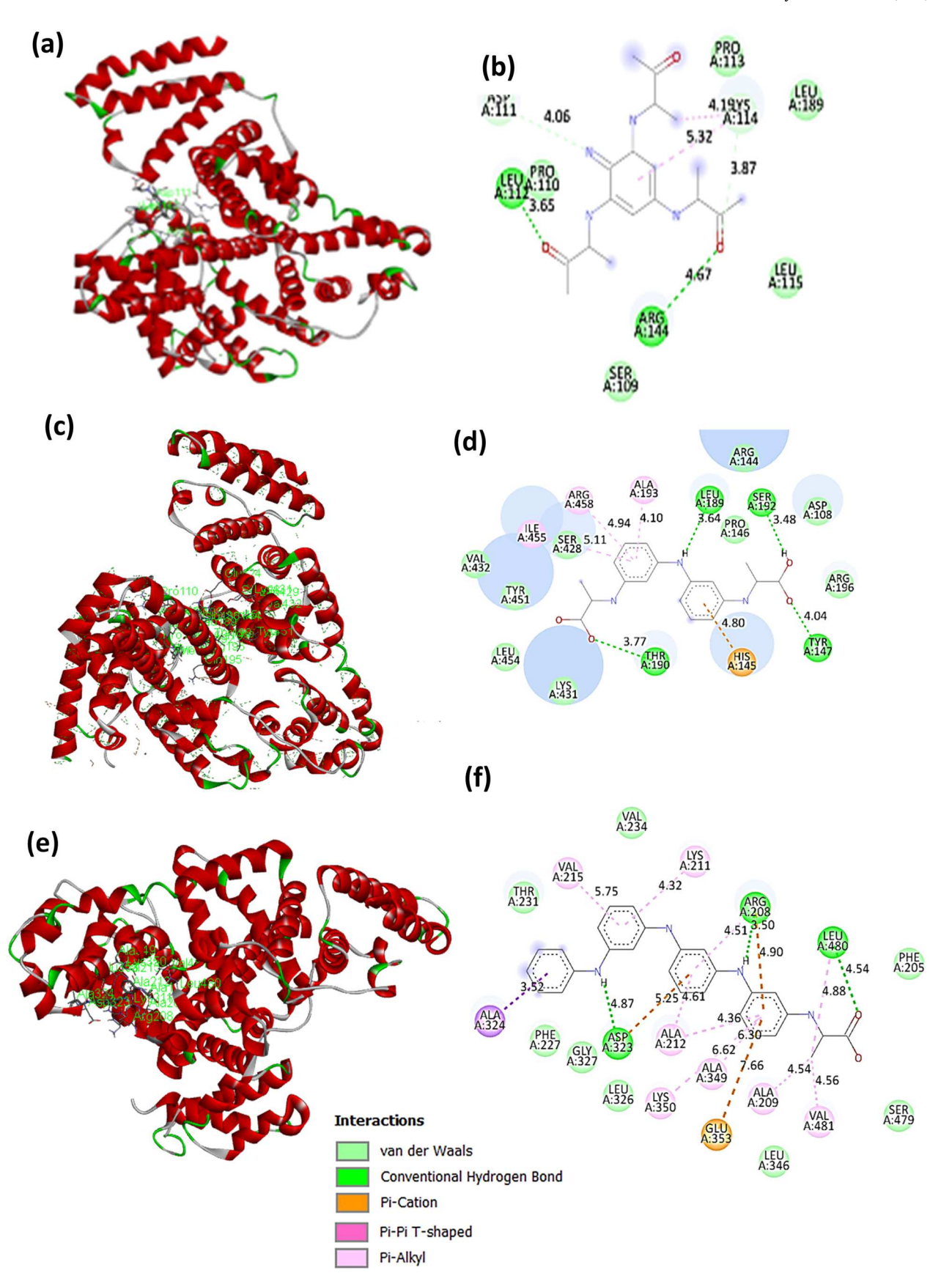


Fig. 8. (a) 3D view of Ala-PANI/80–20-BSA, (b) 2D view of Ala-PANI/80–20-BSA, (c) 3D view of Ala-PANI/50–50-BSA, (d) 2D view of Ala-PANI/50–50-BSA, (e) 3D view of Ala-PANI/20–80-BSA, (f) 2D view Ala-PANI/20–80-BSA.

Table 3Estimated binding energies obtained from docking results.

Complexes	Binding Energy (kJ mol ⁻¹)	List of amino acids involved in binding	Type of Interaction	Distance (Å)
BSA complexe	s			
Ala-PANI/	-3.74	Arg144	Hydrogen Bond	4.67
80-20-BSA		Asp111	Van der Waal	4.06
		Leu112	Hydrogen Bond	3.65
		Lys114	Van der Waal	3.87
Ala-PANI/	-8.43	Ala193	Pi-Pi T-Shaped	4.10
50-50-BSA		Arg458	Pi-Pi T-Shaped Pi-Cation	4.94
		His145 Ile455	Pi-Cation Pi-Alkyl	4.80 5.11
		Leu189	Hydrogen Bond	3.64
		Ser192	Hydrogen Bond	3.48
		Thr190	Hydrogen Bond	3.77
		Tyr147	Hydrogen Bond	4.04
Ala-PANI/	-10	Ala209	Pi-Alkyl	4.29
20-80-BSA		Ala212	Pi-Alkyl	4.19
				4.41
		Ala324	Pi-Sigma	3.53
		Ala349	Pi-Alkyl	4.84
		Arg208	Hydrogen Bond	2.69
		Asp323	Hydrogen Bond	2.75
		Glu353	Pi-Ionic	4.96
		Lys211	Pi-Alkyl	4.84
		Lys350	Pi-Alkyl	5.38
		Leu480 Val215	Hydrogen Bond Pi-Alkyl	2.65 5.75
		Val481	Pi-Alkyl Pi-Alkyl	4.56
HSA complexe	es.	Valitoi	1 1-211Ky1	4.50
Ala-PANI/	-4.69	Arg117	Pi-Alkyl	4.76
80-20-HSA		Arg186	Pi-Alkyl	4.64
		His146	Hydrogen Bond	1.70
		Leu115	Pi-Alkyl	5.37
		Lys519	Hydrogen Bond	2.18
		Met123	Pi-Alkyl	5.18
Ala-PANI/	-8.08	Ala191	Pi-Alkyl	4.28
50-50-HSA		Ala194	Pi-Alkyl	3.49
		Asp108	Hydrogen Bond	3.83
		Arg197 Gln459	Pi-Alkyl Pi-Sigma	6.25 4.74
		His146	Pi-Alkyl	4.74
		Lys190	Hydrogen Bond	5.26
		Lys432	Hydrogen Bond	4.38
		Pro147	Pi-Alkyl	4.45
		Tyr452	Hydrogen Bond	5.04
		Tyr148	Hydrogen Bond	4.60
Ala-PANI/ 20–80-HSA	-9.61	Ala191	Pi-Alkyl	4.23
		Ala194	Pi-Sigma	3.43
		Arg197	Pi-Alkyl	5.25
		Asn429	Unfavourable Donor-Donor	4.87
		Gln459	Hydrogen Bond	2.93
		His146	Van der Walls	5.32
		Lys190	Hydrogen Bond	4.03
		Ser193	Hydrogen Bond	4.52
		Val433	Pi-Alkyl	6.51
		Val455	Pi-Alkyl	5.43
		Tyr452	Pi-Pi Stacked	5.12

Ala-PANI/20–80-BSA, Fig. 6(e). The $\rm K_a$ value was calculated to be 8.2 \times 10⁶ LM $^{-1}$ with binding sites equal to 0.5 for Ala-PANI/80–20-HSA and 8.11 \times 10⁶ LM $^{-1}$ for Ala-PANI/50–50-BSA with binding sites equal to 0.9. For Ala-PANI/20–80-HSA, the binding constant was computed to be 8.7 \times 10⁶ LM $^{-1}$ with binding sites equal to 1, Fig. 7(e). The high binding constant values were attributed to the presence of amide groups that facilitated hydrophobic binding as well as electrostatic binding. The studies confirmed that the quenching of BSA/HSA by Ala-PANI was static in nature and took place via the formation of an intermolecular complex. The quenching rate and binding constant values were found to be highest for Ala-PANI/20–80-BSA and Ala-PANI/20–80-HSA.

The 3D docking view and 2D view of Ala-PANI/80–20-BSA Fig. 8(a),

(b) showed hydrogen bond interaction between -NH and Arg144 with a bond length of 4.67 Å. Another hydrogen bond was observed with Leu112 having a bond length of 3.65 Å, Fig. 8(a), (b), while a Vander Waals interaction was noticed between Asp111 and Leu112 having bond lengths equal to 4.06 Å ad 3.87 Å, Table 3. The binding energy was computed to be -3.74 kJ/mol. For Ala-PANI/50–50-BSA, Fig. 8(c), (d) hydrogen bond interaction was observed with Leu189, Ser192, Thr190 and Tyr147 having bond lengths equal to 3.64 Å, 3.48 Å, 3.77 Å and 4.04 Å respectively. The π - π 'T shaped' bonds were formed with Ala193 and Arg458 with bond lengths equal to 4.10 Å and 4.94 Å. The binding energy was calculated to be -8.43 kJ/mol. For Ala-PANI/20–80-BSA, Fig. 8(e), (f), hydrogen bonding took place between NH of PANI and Arg208, Asp323 with bond length equal to 2.69 Å and 2.75 Å respectively. Several π -alkyl bonds were noticed with Ala349, Lys211, Lys350, Val215, Val481 and the binding energy was computed to be highest around - 10 kJ/mol. The results confirmed that hydrogen bonds and π -alkyl bonds were dominant in the binding process which caused higher binding energy.

The 3D docking view and 2D view of Ala-PANI/80–20-HSA Fig. 9(a), (b) showed hydrogen bond interaction between -NH and His146 with a bond length of 1.70 Å and with Lys519 having a bond length of 2.18 Å, Table 3. The π -alkyl interactions were found with Arg117, Arg186 and Met123. The binding energy was computed to be $-4.69 \, \text{kJ/mol}$. For Ala-PANI/50-50-HSA, Fig. 9(c), (d), hydrogen bond interaction was observed with Asp108, Lys190, Lys432, Tyr452 and Tyr148. The π -alkyl interactions were noticed with Ala191, Ala194, His146, Pro147 and Arg197 and π -sigma interactions were found with Gln459. The binding energy was computed to be -8.08 kJ/mol. For Ala-PANI/20–80-HSA, Fig. 9(e), (f), hydrogen bonds were found between NH of PANI and Gln459, Lys190, Ser193 with bond length equal to 2.93 Å, 4.03 Å and 4.52 Å respectively. There were several π -alkyl bonds noticed with Ala191, Arg197, Val433, Val455, while Ala194 revealed π -sigma bond formation. The binding energy was computed to be - 9.6 kJ/ mol. The results confirmed that hydrogen bonds and π -alkyl/sigma bonds were dominant in the binding process and led to higher binding energy.

5. Conclusion

Alanine modified PANI was synthesized and investigated by experimental as well as theoretically studies. Viscosity average molar mass measurements confirmed the formation of oligomers and hence for computations studies, the geometries were optimized by taking 4 units of Ala and 1 units of aniline for Ala-PANI/80-20, 2 units each of Ala and aniline for Ala-PANI/50-50, and 1 unit of Ala and 4 units of aniline for Ala-PANI/20-80. The experimental and the theoretical IR as well as UV-vis spectra for the Ala incorporated PANI polymers were in close agreement and thus confirmed the geometry optimized structures. The band gap was calculated to be 2.63 eV, 4.84 eV and 2.96 eV for Ala-PANI/80-20, Ala-PANI/50-50 and Ala-PANI/20-80 respectively. The RLS profiles indicated formation of aggregates and the intensities were found to be highest for Ala-PANI-20/80. Circular dichroism showed that the structure of BSA was predominantly α -helical even after binding with the oligomers. The oligomers quenched the fluorescence of BSA and HSA confirming high binding affinity with the proteins. The possible binding modes were further established by molecular docking and showed that the hydrogen bonds and van der Waals forces played a major role in Ala-PANI-BSA/HSA binding. The molecular docking results were in good agreement with experimental results This study is of immense significance in understanding the interaction of Ala-PANI oligomers with BSA as well as HSA at the molecular level and holds potential application in biomedical and pharmaceutical research.

CRediT authorship contribution statement

Ufana Riaz was responsible for conceptualization and data curation; Nuzhat Nabi carried out the spectral and morphological investigations

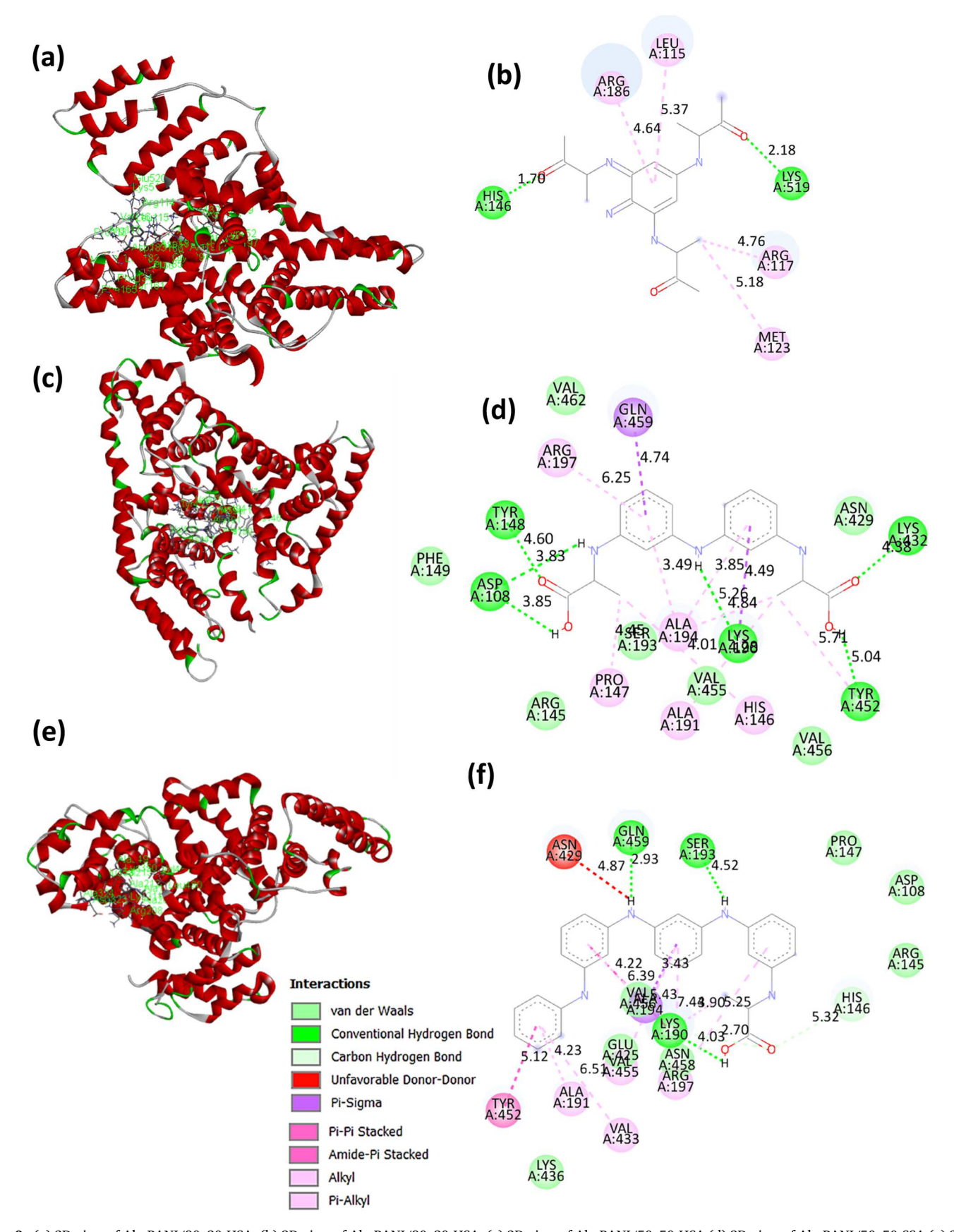


Fig. 9. (a) 3D view of Ala-PANI/80–20-HSA, (b) 2D view of Ala-PANI/80–20-HSA, (c) 3D view of Ala-PANI/50–50-HSA, (d) 2D view of Ala-PANI/50–50-SSA, (e) 3D view of Ala-PANI/20–80-HSA, (f) 2D view Ala-PANI/20–80-HSA.

along with the experimental work; Faith R Nwanze carried out the computational studies and Fei Yan was responsible for funding acquisition and editing.

Declaration of Competing Interest

The authors declare that they have no known competing financial interests or personal relationships that could have appeared to influence the work reported in this paper.

Data Availability

No data was used for the research described in the article.

Acknowledgement

The authors wish to acknowledge National Science Foundation (Award # 2122044), the NSF PREM for Hybrid Nanoscale Systems between NCCU and Penn State for providing financial assistance.

Appendix A. Supporting information

Supplementary data associated with this article can be found in the online version at doi:10.1016/j.synthmet.2022.117248.

References

- [1] B.S. Hudson, Myth and reality, Polyacetylene Mater. 11 (2) (2018) 242.
- [2] P. Zarrintaj, Z. Ahmadi, H. Vahabi, F. Ducos, M. Reza Saeb, M. Mozafari, Polyaniline in retrospect and prospect, Mater. Today Proc. 5 (7) (2018) 15852–15860.
- [3] S. Jadoun, D.S. Rathore, U. Riaz, N.P. Chauhan, Tailoring of conducting polymers via copolymerization – a review, Eur. Polym. J. 155 (2021), 110561.
- [4] S. Jadoun, A. Verma, S.M. Ashraf, U. Riaz, A short review on the synthesis, characterization, and application studies of poly(1-naphthylamine): a seldom explored polyaniline derivative, Colloid Polym. Sci. 295 (9) (2017) 1443–1453.
- [5] J. Kashyap, S. Gautam, S.M. Ashraf, U. Riaz, Synergistic performance of sonolytically synthesized poly(1–naphthylamine)/Tio 2 nanohybrids: degradation studies of amido black-10b dye, ChemistrySelect 3 (42) (2018) 11926–11934.
- [6] N. Singh, P. Kumar, R. Kumar, Ü. Riaz, Ultrasound-assisted polymerization of dyes with phenylenediamines: Facile method to design polymeric photosensitizers with enhanced singlet oxygen generation characteristics and anticancer activity, Ind. Eng. Chem. Res. 58 (31) (2019) 14044–14057.
- [7] S. Jadoun, L. Biswal, U. Riaz, Tuning the optical properties of poly(o-Phenylenediamine-Co-Pyrrole) via template mediated copolymerization, Des. Monomers Polym. 21 (1) (2018) 75–81.
- [8] N. Singh, E.S. Aazam, U. Riaz, Synthesis and characterization of lawsone incorporated singlet oxygen generating conjugated polymers: experimental and computational studies, J. Mol. Struct. 1240 (2021), 130533.
- [9] J. Zia, F. Fatima, U. Riaz, A comprehensive review on the photocatalytic activity of polythiophene-based nanocomposites against degradation of organic pollutants, Catal. Sci. Technol. 11 (20) (2021) 6630–6648.

- [10] J. Zia, E.S. Aazam, U. Riaz, Synthesis of nanohybrids of polycarbazole with α-mno2 derived from brassica oleracea: a comparison of photocatalytic degradation of an antibiotic drug under microwave and UV irradiation, Environ. Sci. Pollut. Res. 27 (19) (2020) 24173–24189.
- [11] J. Zia, M. Riyazuddin, E.S. Aazam, U. Riaz, Rapid catalytic degradation of amoxicillin drug using ZnFe2O4/PCZ nanohybrids under microwave irradiation, Mater. Sci. Eng.: B 261 (2020), 114713.
- [12] F. Kazemi, S.M. Naghib, Y. Zare, K.Y. Rhee, Biosensing applications of polyaniline (Pani)-based nanocomposites: a review, Polym. Rev. 61 (3) (2020) 553–597.
- [13] Q.N. Al-Haidary, A.M. Al-Mokaram, F.M. Hussein, A.H. Ismail, Development of polyaniline for sensor applications: a review, J. Phys.: Conf. Ser. 1853 (1) (2021), 012062
- [14] A. Dinu, C. Apetrei, A review of sensors and biosensors modified with conducting polymers and molecularly imprinted polymers used in electrochemical detection of amino acids: phenylalanine, tyrosine, and tryptophan, Int. J. Mol. Sci. 23 (3) (2022) 1218.
- [15] A. Verma, P. Kumar, U. Riaz, Biodegradable polymers in controlled drug delivery systems, Appl. Encapsulation Control. Release (2019) 131–143.
- [16] A. Verma, U. Riaz, Synthesis, characterization and in vitro drug release studies of sonolytically intercalated poly(O-Anisidine)/montmorillonite nanocomposites, Macromol. Res. 27 (2) (2018) 140–152.
- [17] U. Riaz, S. Ashraf, Corrosion protective coatings based on electroactive polymers, Corros. Mater. Oil Gas. Ind. (2013) 395–414.
- [18] U. Riaz, C. Nwaoha, S.M. Ashraf, Recent advances in corrosion protective composite coatings based on conducting polymers and natural resource derived polymers, Prog. Org. Coat. 77 (4) (2014) 743–756.
- [19] M. Mattioli-Belmonte, G. Giavaresi, G. Biagini, L. Virgili, M. Giacomini, M. Fini, F. Giantomassi, D. Natali, P. Torricelli, R. Giardino, Tailoring biomaterial compatibility: in vivo tissue response versus in vitro cell behavior, Int. J. Artif. Organs 26 (12) (2003) 1077–1085.
- [20] S. Battistoni, et al., International Conference on Memristive Systems (MEMRISYS) 2015, IEEE, 2015.
- [21] M. Akhtar, A. Tahir, S. Zulfiqar, F. Hanif, M.F. Warsi, P.O. Agboola, I. Shakir, Ternary hybrid of polyaniline-alanine-reduced graphene oxide for electrochemical sensing of heavy metal ions, Synth. Met. 265 (2020), 116410.
- [22] J. Han, Y.S. Chi, Vibrational and electronic spectroscopic characterizations of amino acid-metal complexes, J. Korean Soc. Appl. Biol. Chem. 53 (6) (2010) 821–825.
- [23] U. Riaz, S.M. Ashraf, S. Jadoun, V. Budhiraja, P. Kumar, Spectroscopic and biophysical interaction studies of water-soluble dye modified poly(ophenylenediamine) for its potential application in BSA detection and bioimaging, Sci. Rep. 9 (1) (2019) 8544.
- [24] U. Riaz, S.M. Ashraf, S. Aleem, V. Budhiraja, S. Jadoun, Microwave-assisted green synthesis of some nanoconjugated copolymers: characterisation and fluorescence quenching studies with bovine serum albumin, New J. Chem. 40 (5) (2016) 4643–4653.
- [25] N. Singh, R. Ali, S.M. Ashraf, A. Rub, U. Riaz, Experimental and computational studies of novel sudan-I dye modified conjugated oligomers: efficient 1O2 generation and antileishmanial characteristics, Mater. Sci. Eng. B 265 (2021), 114993
- [26] N. Singh, R. Ali, S.M. Ashraf, A. Rub, U. Riaz, Experimental and computational studies of novel sudan-I dye modified conjugated oligomers: efficient 1O2 generation and antileishmanial characteristics, Mater. Sci. Eng. B 265 (2021), 114993.
- [27] J. Zhang, W. Chen, B. Tang, W. Zhang, L. Chen, Y. Duan, Y. Zhu, Y. Zhu, Y. Zhu, Y. Zhang, Interactions of 1-hydroxypyrene with bovine serum albumin: insights from multispectroscopy, docking and molecular dynamics simulation methods, RSC Adv. 6 (28) (2016) 23622–23633.